Coupling of magnetism and Dirac fermions in YbMnSb$_2$

Xiao Hu,[1] Aashish Sapkota,[1,2] Zhixiang Hu,[1,3] Andrei T. Savici,[4] Alexander I. Kolesnikov,[4] John M. Tranquada,[1] Cedomir Petrovic,[1,3] and Igor A. Zaliznyak[1,*]

[1]*Condensed Matter Physics and Materials Science Division,*
Brookhaven National Laboratory, Upton, NY 11973, USA
[2]*Ames National Laboratory, U.S. DOE, Department of Physics and Astronomy, Iowa State University, Ames, Iowa 50011, USA*
[3]*Department of Material Science and Chemical Engineering,*
Stony Brook University, Stony Brook, NY, 11790, USA
[4]*Neutron Scattering Division, Oak Ridge National Laboratory, Oak Ridge, TN 37831, USA*

(Dated: May 16, 2023)

We report inelastic neutron scattering measurements of magnetic excitations in YbMnSb$_2$, a low-carrier-density Dirac semimetal in which the antiferromagnetic Mn layers are interleaved with Sb layers that host Dirac fermions. We observe a measurable broadening of spin waves, which is consistent with substantial spin-fermion coupling. The spin wave damping, γ, in YbMnSb$_2$ is roughly twice larger compared to that in a sister material, YbMnBi$_2$, where an indication of a small damping consistent with theoretical analysis of the spin-fermion coupling was reported. The inter-plane interaction between the Mn layers in YbMnSb$_2$ is also much stronger, suggesting that the interaction mechanism is rooted in the same spin-fermion coupling. Our results establish the systematics of spin-fermion interactions in layered magnetic Dirac materials.

Introduction. Dirac semimetals remain at the forefront of research on topological materials because of the fascinating quantum electronic phenomena they exhibit and of their potential technological applications [1–6]. In these materials, the characteristic linear electronic dispersion leads to novel behaviors such as spin-polarized transport [3], suppression of back-scattering due to spin-momentum locking [7–9], the chiral anomaly [10–12], impurity-induced resonant states, and the anomalous quantum Hall effect [4–6, 13, 14].

Among different types of Dirac semimetals, the family of 112 ternary pnictogens with the general formula $A/R\mathrm{Mn}X_2$ (A = Ca, Sr; R = Yb, Eu; X = Bi, Sb) have attracted particular attention due to the combination of highly anisotropic Dirac dispersion in quasi-2D square nets of X atoms and strongly correlated magnetism of Mn [5, 15–24]. These materials feature a common layered structure in which the X layers hosting itinerant Dirac charge carriers are separated by strongly-correlated insulating Mn-X layers. Both the inter-layer charge transport and the magnetic correlations between the Mn layers require that Dirac carriers are coupled to strongly-correlated Mn electrons. Therefore, these materials have become a fertile playground for investigating the interaction of the conduction Dirac electrons with the local-spin magnetic Mn-X sublattice, i.e. spin-Dirac fermion coupling [5, 15, 17, 25, 26].

Previous inelastic neutron scattering (INS) measurements on (Sr, Ca)MnBi$_2$ reported no indication of such coupling because anomalous broadening of magnetic excitations found in itinerant magnets was not observed [26, 27]. Yet, the out-of-plane antiferromagnetism in SrMnBi$_2$ and ferromagnetism in CaMnBi$_2$ [26] clearly indicate the presence of inter-layer interaction between magnetic Mn^{2+} ions, which inevitably involves Dirac electrons in the interweaving Bi square nets. A detailed analysis of high-resolution INS measurements of magnetic excitations in YbMnBi$_2$ led us to discover a signature of spin-Dirac fermion coupling in this material [28]. We found a small but distinct broadening of spin wave dispersion, both for the in-plane and the out-of-plane directions. For $T < T_N$, the broadening is weakly dependent on temperature and is nearly $\boldsymbol{Q}$-independent. With magnon-magnon and magnon-phonon scattering suppressed, at $T \ll T_N, \Theta_D$ (Θ_D is Debye temperature) the decay of magnons into electron-hole excitations is the leading mechanism for the observed spin-wave damping. This effect can be very large in itinerant magnets, but for Dirac electrons it is greatly suppressed due to their small density of states. By comparing the observed spin wave damping with theoretical model of Dirac fermions coupled to spin waves, we found a very substantial spin-fermion coupling parameter, $g \approx 1.0$ eV$^{3/2}$ Å (cf Eq. 3 in [28]).

In order to establish the systematics of spin-fermion coupling in the 112 family of Dirac semimetals and further elucidate its properties, we carried out INS measurements on a sister material, YbMnSb$_2$, where heavier Bi is substituted with the lighter Sb, thus reducing the spin-orbit coupling (SOC) and potentially softening Dirac dispersion. YbMnSb$_2$ crystallizes in the same $P4/nmm$ space group as YbMnBi$_2$ (Yb^{2+} is non-magnetic), but weaker SOC is more favorable for stronger coupling of the massless Dirac fermions to magnons [21, 29, 30]. Angle-resolved photoemission, Shubnikov-de-Haas oscillations [23], and optical spectroscopy [31], combined with the electronic band structure calculations, indicate a nearly nodal-line anisotropic Dirac dispersion near the Fermi level, similar to that in YbMnBi$_2$ (see Fig. 4 in [28]). From the analysis of well-defined magnetic excitations observed in our experiments, we extract a damping parameter consistent with appreciable broadening of spin waves and substantial spin-fermion coupling. The spin wave damping and the inter-layer interaction in YbMnSb$_2$ are significantly stronger than those in YbMnBi$_2$. We note that for our measurements at low temperature of ≈ 5.5 K, damping induced by spin-phonon coupling is greatly suppressed and thus our observations corroborate the idea that it originates from cou-

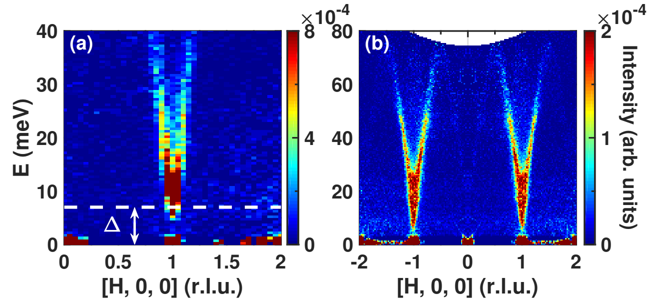

FIG. 1. **Spin waves in YbMnSb$_2$ in the antiferromagnetic state at $T = 5.5(5)$ K.** Inelastic neutron scattering spectra measured with incident energies $E_\mathrm{i} = 50$ (a) and 100 (b) meV showing the dispersion along $[H, 0, 0]$ direction. Data bin sizes in H and K are ± 0.025. The data in (a) have bin size ± 0.06 in L and were averaged over L = integers with $L \in [-5, 5]$; in (b) were averaged over the continuous interval $L \in [-6, 6]$; the L-integrated data differs from narrow slices in panel (a) and Fig. 2 in that it allows to better visualize the high energy spin waves, which are weakly sensitive to dispersion along L. The value of Δ is given in Table I. For fitting, only the data measured with $E_\mathrm{i} = 100$ meV are used, as shown in Fig 2. The Gaussian elastic incoherent spectrum obtained by fitting the Q-averaged elastic intensity was subtracted.

pling to Dirac fermions.

Experimental Details. Single crystals of YbMnSb$_2$ were grown from Sb flux using the method described in [24]. YbMnSb$_2$ orders antiferromagnetically below $T_\mathrm{N} \approx 345$ K, with an ordered moment of $3.48\mu_\mathrm{B}$ at 2 K [30]. INS measurements were performed at the SEQUOIA spectrometer at the Spallation Neutron Source, Oak Ridge National Laboratory. Three single crystals with a total mass of ≈ 1.8 g were co-aligned in the $(H, 0, L)$ horizontal scattering plane. The measurements were carried out with incident energies $E_\mathrm{i} = 50$, 100, and 150 meV at $T = 5.5(5)$ K by rotating the sample about the vertical axis in $1\,\mathrm{deg}$ steps over a $270\,\mathrm{deg}$ range. Throughout the paper, we index the momentum transfer, $\boldsymbol{Q} = (H, K, L)$ in reciprocal lattice units (r.l.u) of the $P4/nmm$ lattice, $a = b = 4.31(2)$ Å, $c = 10.85(1)$ Å [23, 24, 31]. The data reduction and histogramming to rectangular grid were performed using the MANTID package [32] and the MDNorm algorithm [33] (see supplementary information for details [34]).

Results and Analysis. Figure 1 (a),(b) present inelastic neutron scattering spectra for YbMnSb$_2$ in the antiferromagnetic (AFM) phase at $T = 5.5(5)$ K, which reveal the spin wave dispersion along the $[H, 0, 0]$ symmetry direction. The well-defined spin waves are consistent with the local-moment description and emerge above the AFM wave vector $\boldsymbol{Q}_\mathrm{AFM} = (\pm 1, 0, 0)$, as expected for a Néel-type magnetic order in YbMnSb$_2$ [30]. Figure 1(a) shows high-resolution data, which clearly demonstrate the presence of a spin-gap, $\Delta \approx 7$ meV, resulting from the uniaxial anisotropy. It also suggests that the spin wave spectrum is slightly blurred along the energy axis, indicating the presence of damping. The spin-wave dispersion bandwidth along $(H, 0, 0)$, $W = E_{\boldsymbol{Q}=(1.5,0,0)} \gtrsim 70$ meV, is significantly larger than the values measured in YbMnBi$_2$, CaMnBi$_2$, and SrMnBi$_2$ [27, 28], indicating stronger in-plane exchange coupling, J. In spin wave theory, $W \sim J$ and $\Delta \sim \sqrt{DJ}$, where D is the uniaxial anisotropy constant. Despite larger J, the anisotropy gap in YbMnSb$_2$ is smaller compared to $\Delta \approx 9$ meV in YbMnBi$_2$ [28], which is consistent with the weaker SOC of the lighter Sb atoms and hence smaller anisotropy, D.

In order to quantify the interactions and elucidate the presence of damping, we perform quantitative analysis of the measured intensity using an effective spin Hamiltonian, $H = \Sigma_{ij} J_{ij} \mathbf{S}_i \cdot \mathbf{S}_j + D\Sigma_i (S_i^z)^2$, where J_{ij} includes the interaction between the nearest and next-nearest neighbors in the ab plane (J_1 and J_2) and nearest neighbors along the c axis

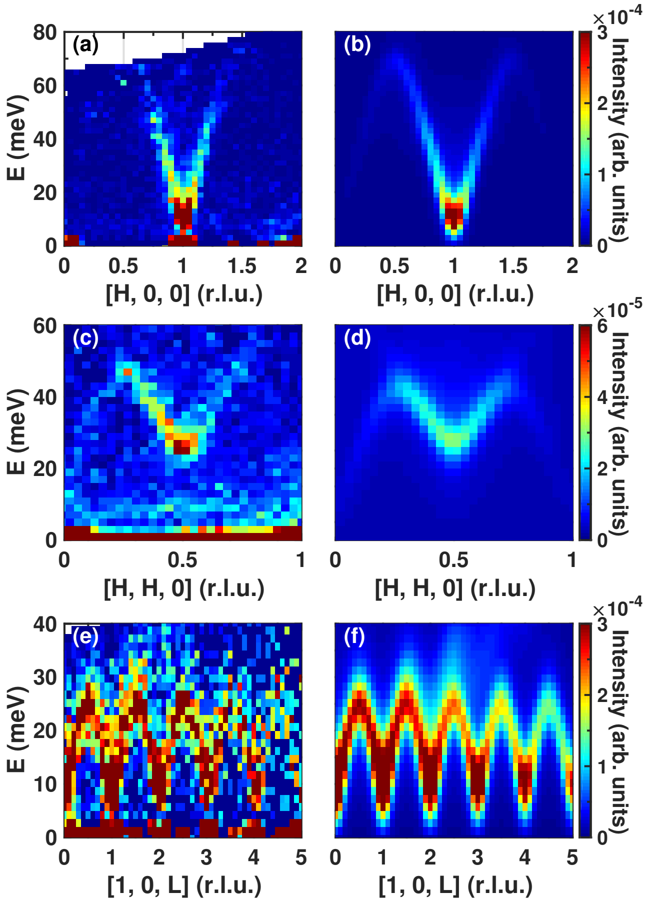

FIG. 2. **Measured and fitted spin wave spectra of YbMnSb$_2$.** The INS spectra measured with $E_\mathrm{i} = 100$ meV at $T = 5.5(5)$ K along three symmetry directions, $[H, 0, 0]$ (a), $[H, H, 0]$ (c), and $[1, 0, L]$ (e). Data bin sizes in (a) are $\pm 0.025, \pm 0.025, \pm 0.06$ in H, K, L, respectively, in (c) are $\pm 0.0175, \pm 0.035, \pm 0.1$ in $(H, H, 0)$, $(-H, H, 0)$, L, respectively, and in (e) are $\pm 0.025, \pm 0.025, \pm 0.05$ in H, K, L, respectively. The spectra in (a) and (c) were averaged for integer L in the range $|L| \leq 5$. (b), (d), and (f) are the INS spectra calculated using Eqs. (1) corrected for the instrument resolution and with the fitted parameters listed in Table I (see [34] for details).

(J_c). As above, D quantifies the uniaxial anisotropy for the Mn^{2+} spins corresponding to an easy axis along the c direction ($D < 0$). In order to account for the spin-wave damping, i.e. the finite spin wave lifetime, we use a damped-harmonic-oscillator (DHO) representation of the dynamical spin correlation function, $S(\boldsymbol{Q}, E)$ [28],

$$S(\boldsymbol{q}+\boldsymbol{Q}_{\mathrm{AFM}}, E) = S_{\mathrm{eff}}\frac{1}{\pi}\frac{2(A_{\boldsymbol{q}}-B_{\boldsymbol{q}})}{1-e^{-E/k_{\mathrm{B}}T}} \times A\frac{\gamma E}{\left[E^2-E_{\boldsymbol{q}}^2\right]^2+(\gamma E)^2} . \qquad (1)$$

Here, γ is the damping parameter (Lorentzian FWHM for underdamped DHO), k_{B} is the Boltzmann constant, S_{eff} is the effective fluctuating spin, and prefactor A ensures that the DHO spectral function is normalized to 1 (for $(T,\gamma) \to 0$, $A \to 1$) [34]. At $T = 5.5(5)$ K $\ll T_N$, spin wave theory gives $A_{\boldsymbol{q}} = 2S[2J_1 - 2J_2[\sin^2(\pi H) + \sin^2(\pi K)] - 2J_c\sin^2(\pi L) - D]$, $B_{\boldsymbol{q}} = 4SJ_1\cos(\pi H)\cos(\pi K)$, and $E_{\boldsymbol{q}}^2 = A_{\boldsymbol{q}}^2 - B_{\boldsymbol{q}}^2$. The lowest energy for the $[H,H,0]$ direction, $E_{[0.5,0.5,0]} = 2S(2J_1 - 4J_2 + |D|)$, is the exchange gap, while that along $[H,0,0]$, $E_{[1,0,0]} = 2S\sqrt{(4J_1 + |D|)|D|}$, is the anisotropy gap.

We fit the data using Eq. (1) convoluted with the instrumental resolution function including the finite $(\boldsymbol{Q}, E)$ bin size effects [28]. Account for the wave vector resolution is important because the energy line width at each $\boldsymbol{Q}$ is determined by the convolution, which causes the local averaging over the dispersion [34]. We performed global fits of the 2D energy and wave vector slices shown in Fig. 2(a),(c),(e) using a single damping parameter, γ, as well as individual fits of constant-$\boldsymbol{Q}$ cuts with individual $\gamma(\boldsymbol{Q})$. The INS intensities calculated using the fitted values and the resolution corrected Eq. (1) are shown in Fig. 2(b),(d),(f). The fit results are summarized in Fig. 3.

The major result of our analysis is the substantial spin wave damping parameter, $\gamma \approx 7.0$ meV, which in YbMnSb$_2$ is nearly twice larger than that in YbMnBi$_2$ [28]. As in YbMnBi$_2$, the damping is roughly $\boldsymbol{Q}$-independent. Figure 3 shows that the γ values obtained by fitting the individual 1D constant-$\boldsymbol{Q}$ cuts (symbols) fall within about twice the instrumental energy resolution, E_{res}, of the 2D global-fitted γ value (horizontal dashed line), which closely agrees with the average of $\gamma(\boldsymbol{Q})$. Note, that the absence of $\gamma(\boldsymbol{Q})$ minima near the gap positions, [1, 0, 0] in Fig. 3(b) and [1, 0, 1] in Fig. 3(d), where the dispersion is flat and $\boldsymbol{Q}$-resolution effects are least important, validates our account for the resolution and corroborates that the observed spin wave broadening is intrinsic. In order to further confirm this, we verified that assuming $\gamma \approx 0$ leads to noticeably inferior quality fits (see Fig. S3 in [34]).

Discussions and Conclusions. Understanding the coupling between highly localized magnetic moments of strongly correlated Mn electrons and the Dirac electrons originating in pnictogen (Bi, Sb) layers of $A/R\mathrm{Mn}X_2$ materials presents an important but challenging problem. The layered structure of these systems, where magnetic layers are sandwiched between the layers with the itinerant Dirac electrons, suggests that inter-layer magnetic interactions must involve Dirac fermions. This is further corroborated by observations of a subtle resistivity anomaly at T_N in $A\mathrm{MnBi}_2$ (A = Ca, Sr) [26], indicating a coupling between the Dirac bands and the magnetic ground state. Other studies [16, 35], however, do not report the anomaly. Similarly, no evidence that the magnetic dynamics are influenced by the Dirac/Weyl fermions was obtained from the spin wave analyses of the INS measurement of magnetic excitations which did not consider spin wave damping [27, 36, 37].

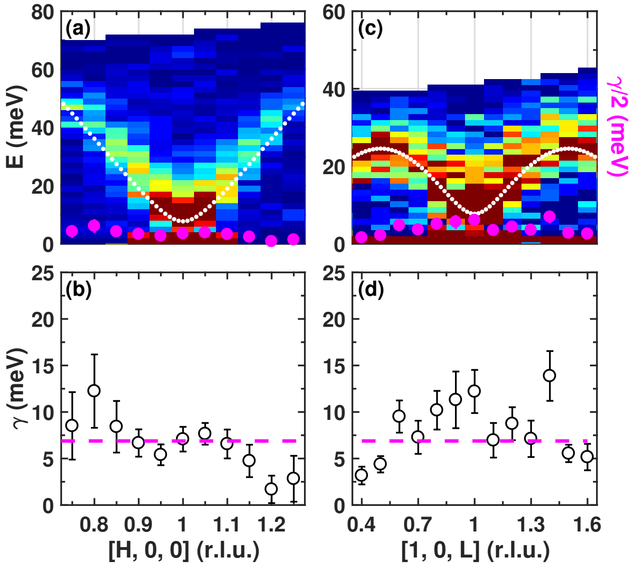

FIG. 3. **Spin wave dispersion and damping parameter in YbMnSb$_2$ at 5.5(5) K.** The white dotted lines on top of the INS intensity in (a),(c) illustrate the dispersion obtained using the parameters in Table I without damping. The underdamped spin waves exist where $E_{\boldsymbol{q}} > \gamma/2$ (magenta symbols). The symbols show damping obtained by fitting the 1D constant-$\boldsymbol{Q}$ cuts along $[H,0,0]$, (a),(b), and $[1,0,L]$, (c),(d), directions with the resolution corrected Eq. (1). The magenta dashed lines represent the γ value from Table I obtained from the global 2D fit. Error bars show one standard deviation.

TABLE I. Exchange coupling, uniaxial anisotropy, and damping parameters for YbMnSb$_2$ obtained from fitting two-dimensional data shown in Fig. 2 and those in YbMnBi$_2$ from Ref. 28.

	YbMnBi$_2$[28]	YbMnSb$_2$
SJ_1 (meV)	25.9 ± 0.2	28.1 ± 0.1
SJ_2 (meV)	10.1 ± 0.2	10.7 ± 0.1
SJ_c (meV)	-0.130 ± 0.002	-0.597 ± 0.023
SD (meV)	-0.20 ± 0.01	-0.13 ± 0.01
Δ (meV)	9.1 ± 0.2	7.7 ± 0.4
γ (meV)	3.6 ± 0.2	6.9 ± 0.4

The reason for the difficulty of experimentally observing the manifestations of spin-fermion coupling with Dirac electrons is that the linear Dirac dispersion has a low density of states and therefore their effect on spin wave excitations is weak. Nevertheless, a thorough analysis of spin wave spectra measured by INS in YbMnBi$_2$, similar to the one presented here, did find a non-negligible spin wave damping, $\gamma \approx 3.6$ meV (Table I) [28]. A comparison with the theoretical model showed that albeit small, this damping is a signature of a very substantial spin-fermion coupling.

The results of our analysis presented in Table I show that the damping parameter in YbMnSb$_2$ is about twice larger than that in YbMnBi$_2$, while the inter-layer interaction is roughly four times larger in magnitude and the intra-layer interaction J_1 is $\sim 10\%$ larger. In addition to establishing experimental systematics, these quantitative relationships suggest that Dirac charge carriers may in fact participate in mediating all magnetic interactions between Mn moments, both intra- and interplane. In this scenario, it might be instructive to infer functional relationships between $J_{1,2}$, J_c, and γ, such as $J_c \propto \gamma^2$, which comply with the experimental observations and provide experimental guidance for future theories.

In summary, our INS measurements of magnetic excitations in single crystals of Dirac semimetal YbMnSb$_2$ reveal considerable broadening of the antiferromagnetic spin waves at low temperature, $T \approx 5.5$ K$\ll T_N$, which is consistent with substantial spin-fermion coupling in this material. By fitting the measured spin wave spectra to Heisenberg model with easy-axis anisotropy and with finite spin wave lifetime (damping), we extracted the damping parameter, $\gamma = 6.9(4)$ meV, and inter- and intra-layer exchange interactions. Comparison of the obtained model parameters with those in YbMnBi$_2$ and other 112 Dirac materials allows establishing systematic phenomenology of spin-fermion coupling in these systems and suggests that Dirac electrons are involved in the inter-layer spin coupling and might also participate in all magnetic interactions between Mn^{2+} ions. While developing theoretical description of such an RKKY-type coupling via Dirac electrons presents a challenge for the future, our results provide experimental guidance for such theories and an input for predictive theory of the magnetotransport phenomena in this regime.
Note added. While this work was being finalized for publication, a related INS study [38] of YbMnSb$_2$ using triple axis spectroscopy (TAS) appeared. While constraints of instrumental resolution ($\Delta E_{FWHM} \approx 8$ meV) inherent to TAS in the energy range relevant for this study did not allow those authors to explore spin wave damping and resulted in moderately different Hamiltonian parameters (refined by fitting triple axis measurements to the same model as we use here but without damping), the general trends and conclusions reported in [38] support our results. In particular, they support the conclusion that spin-fermion coupling in YbMnSb$_2$ is stronger and more important compared to other 112 systems. It is also noteworthy that half-polarized neutron diffraction reported in [38] confirms the localized, ionic nature of Mn magnetic moments, giving direct experimental support to models of spin-fermion coupling such as proposed in our earlier work [28].

Acknowledgements We gratefully acknowledge discussions with A. Tsvelik and technical assistance from V. Fanelli. This work at Brookhaven National Laboratory was supported by Office of Basic Energy Sciences (BES), Division of Materials Sciences and Engineering, U.S. Department of Energy (DOE), under contract DE-SC0012704. This research used resources at the Spallation Neutron Source, a DOE Office of Science User Facility operated by the Oak Ridge National Laboratory.

---

[*] zaliznyak@bnl.gov

[1] F. Katmis, V. Lauter, F. S. Nogueira, B. A. Assaf, M. E. Jamer, P. Wei, B. Satpati, J. W. Freeland, I. Eremin, D. Heiman, P. Jarillo-Herrero, and J. S. Moodera, Nature **533**, 513 (2016).
[2] H. Masuda, H. Sakai, M. Tokunaga, Y. Yamasaki, A. Miyake, J. Shiogai, S. Nakamura, S. Awaji, A. Tsukazaki, H. Nakao, Y. Murakami, T.-h. Arima, Y. Tokura, and S. Ishiwata, Sci. Adv. **2**, 10.1126/sciadv.1501117 (2016).
[3] M. Khodas, I. A. Zaliznyak, and D. E. Kharzeev, Phys. Rev. B **80**, 125428 (2009).
[4] T. Wehling, A. Black-Schaffer, and A. Balatsky, Advances in Physics **63**, 1 (2014).
[5] K. Wang, D. Graf, H. Lei, S. W. Tozer, and C. Petrovic, Phys. Rev. B **84**, 220401 (2011).
[6] A. Wang, D. Graf, L. Wu, K. Wang, E. Bozin, Y. Zhu, and C. Petrovic, Phys. Rev. B **94**, 125118 (2016).
[7] M. König, S. Wiedmann, C. Brüne, A. Roth, H. Buhmann, L. W. Molenkamp, X.-L. Qi, and S.-C. Zhang, Science **318**, 766 (2007).
[8] D. Hsieh, Y. Xia, D. Qian, L. Wray, J. H. Dil, F. Meier, J. Osterwalder, L. Patthey, J. G. Checkelsky, N. P. Ong, A. V. Fedorov, H. Lin, A. Bansil, D. Grauer, Y. S. Hor, R. J. Cava, and M. Z. Hasan, Nature **460**, 1101 (2009).
[9] Y. S. Hor, P. Roushan, H. Beidenkopf, J. Seo, D. Qu, J. G. Checkelsky, L. A. Wray, D. Hsieh, Y. Xia, S.-Y. Xu, D. Qian, M. Z. Hasan, N. P. Ong, A. Yazdani, and R. J. Cava, Physical Review B **81**, 195203 (2010).
[10] M. Ezawa, Physical Review B **95**, 205201 (2017).
[11] Y.-Y. Lv, X. Li, B.-B. Zhang, W. Y. Deng, S.-H. Yao, Y. B. Chen, J. Zhou, S.-T. Zhang, M.-H. Lu, L. Zhang, M. Tian, L. Sheng, and Y.-F. Chen, Physical Review Letters **118**, 096603 (2017).
[12] V. Aji, Physical Review B **85**, 241101 (2012).
[13] Y. Zhang, Y.-W. Tan, H.-L. Stormer, and P. Kim, Nat. **438**, 201 (2005).
[14] M. Z. Hasan and C. L. Kane, Rev. Mod. Phys. **82**, 3045 (2010).
[15] J. Park, G. Lee, F. Wolff-Fabris, Y. Y. Koh, M. J. Eom, Y. K. Kim, M. A. Farhan, Y. J. Jo, C. Kim, J. H. Shim, and J. S. Kim, Phys. Rev. Lett. **107**, 126402 (2011).
[16] K. Wang, D. Graf, L. Wang, H. Lei, S. W. Tozer, and C. Petrovic, Phys. Rev. B **85**, 041101 (2012).
[17] A. Wang, I. Zaliznyak, W. Ren, L. Wu, D. Graf, V. O. Garlea, J. B. Warren, E. Bozin, Y. Zhu, and C. Petrovic, Phys. Rev. B **94**, 165161 (2016).
[18] A. F. May, M. A. McGuire, and B. C. Sales, Physical Review B **90**, 075109 (2014).
[19] M. Chinotti, A. Pal, W. J. Ren, C. Petrovic, and L. Degiorgi, Phys. Rev. B **94**, 245101 (2016).
[20] G. Lee, M. A. Farhan, J. S. Kim, and J. H. Shim, Phys. Rev. B **87**, 245104 (2013).
[21] J. Liu, J. Hu, H. Cao, Y. Zhu, A. Chuang, D. Graf, D. J. Adams, S. M. A. Radmanesh, L. Spinu, I. Chiorescu, and Z. Mao, Scientific Reports **6**, 10.1038/srep30525 (2016).

[22] D. Chaudhuri, B. Cheng, A. Yaresko, Q. D. Gibson, R. J. Cava, and N. P. Armitage, Phys. Rev. B **96**, 075151 (2017).

[23] R. Kealhofer, S. Jang, S. M. Griffin, C. John, K. A. Benavides, S. Doyle, T. Helm, P. J. W. Moll, J. B. Neaton, J. Y. Chan, J. D. Denlinger, and J. G. Analytis, Physical Review B **97**, 045109 (2018).

[24] Y.-Y. Wang, S. Xu, L.-L. Sun, and T.-L. Xia, Physical Review Materials **2**, 021201 (2018).

[25] A. Zhang, C. Liu, C. Yi, G. Zhao, T.-l. Xia, J. Ji, Y. Shi, R. Yu, X. Wang, C. Chen, and Q. Zhang, Nat. Commun. **7**, 13833 (2016).

[26] Y. F. Guo, A. J. Princep, X. Zhang, P. Manuel, D. Khalyavin, I. I. Mazin, Y. G. Shi, and A. T. Boothroyd, Phys. Rev. B **90**, 075120 (2014).

[27] M. C. Rahn, A. J. Princep, A. Piovano, J. Kulda, Y. F. Guo, Y. G. Shi, and A. T. Boothroyd, Phys. Rev. B **95**, 134405 (2017).

[28] A. Sapkota, L. Classen, M. B. Stone, A. T. Savici, V. O. Garlea, A. Wang, J. M. Tranquada, C. Petrovic, and I. A. Zaliznyak, Physical Review B **101**, 041111 (2020).

[29] J. Y. Liu, J. Hu, Q. Zhang, D. Graf, H. B. Cao, S. M. A. Radmanesh, D. J. Adams, Y. L. Zhu, G. F. Cheng, X. Liu, W. A. Phelan, J. Wei, M. Jaime, F. Balakirev, D. A. Tennant, J. F. DiTusa, I. Chiorescu, L. Spinu, and Z. Q. Mao, Nature Materials **16**, 905 (2017).

[30] J.-R. Soh, S. M. Tobin, H. Su, I. Zivkovic, B. Ouladdiaf, A. Stunault, J. A. Rodríguez-Velamazán, K. Beauvois, Y. Guo, and A. T. Boothroyd, Phys. Rev. B **104**, L161103 (2021).

[31] Z. Qiu, C. Le, Z. Liao, B. Xu, R. Yang, J. Hu, Y. Dai, and X. Qiu, Physical Review B **100**, 125136 (2019).

[32] O. Arnold, J. Bilheux, J. Borreguero, A. Buts, S. Campbell, L. Chapon, M. Doucet, N. Draper, R. F. Leal, M. Gigg, V. Lynch, A. Markvardsen, D. Mikkelson, R. Mikkelson, R. Miller, K. Palmen, P. Parker, G. Passos, T. Perring, P. Peterson, S. Ren, M. Reuter, A. Savici, J. Taylor, R. Taylor, R. Tolchenov, W. Zhou, and J. Zikovsky, Nucl. Instr. Meth. Phys. Res. A **764**, 156 (2014).

[33] A. T. Savici, M. A. Gigg, O. Arnold, R. Tolchenov, R. E. Whitfield, S. E. Hahn, W. Zhou, and I. A. Zaliznyak, Journal of Applied Crystallography **55**, 1514 (2022).

[34] See supplementary materials for additional details.

[35] J. He, D. Wang, and G. Chen, Applied Physics Letters **100**, 112405 (2012).

[36] J.-R.Soh, H. Jacobsen, B. Ouladdiaf, A. Ivanov, A. Piovano, T. Tejsner, Z. Feng, H. Wang, H. Su, Y. Guo, Y. Shi, and A. T. Boothroyd, Physical Review B **100**, 144431 (2019).

[37] Z. Cai, S. Bao, W. Wang, Z. Ma, Z.-Y. Dong, Y. Shangguan, J. Wang, K. Ran, S. Li, K. Kamazawa, M. Nakamura, D. Adroja, S.-L. Yu, J.-X. Li, and J. Wen, Physical Review B **101**, 134408 (2020).

[38] S. M. Tobin, J.-R. Soh, H. Su, A. Piovano, A. Stunault, J. A. Rodríguez-Velamazán, Y. Guo, and A. T. Boothroyd, arXiv e-prints 10.48550/arXiv.2302.07007 (2023), 2302.07007 [cond-mat.str-el].

[39] I. A. Zaliznyak and S.-H. Lee, in *Modern Techniques for Characterizing Magnetic Materials*, edited by Y. Zhu (Springer US, 2005) pp. 3–64.

[40] D. L. Abernathy, M. B. Stone, M. J. Loguillo, M. S. Lucas, O. Delaire, X. Tang, J. Y. Y. Lin, and B. Fultz, Rev. Sci. Instrum. **83**, 015114 (2012).